Proceedings of the 2013 International Symposium on Liquid Metal Processing & Casting
Edited by: Matthew J. M. Krane, Alain Jardy, Rodney L. Williamson, and Joseph J. Beaman
TMS (The Minerals, Metals & Materials Society), 2013

A NUMERICAL STUDY ON THE INFLUENCE OF THE FREQUENCY OF THE APPLIED AC CURRENT ON THE ELECTROSLAG REMELTING PROCESS

E. Karimi Sibaki [1], A. Kharicha [1,2], M. Wu [1,2], A. Ludwig [2], H. Holzgruber [3]
B. Ofner [3], M. Ramprecht [3]
[1] Christian Doppler Laboratory for Advanced Process Simulation of Solidification and Melting, Univ. of Leoben, Austria
[2] Chair of Simulation and Modeling of Metallurgical Processes, Univ. of Leoben, Austria
[3] INTECO Special Melting Technologies GmbH, 8600 Bruck/Mur, Austria
Correspondent author: abdellah.kharicha@unileoben.ac.at

Keywords: Electroslag Remelting (ESR), Magnetohydrodynamics (MHD), Solidification, AC Current.

Abstract

Most conventional electroslag remelting (ESR) processes are operated with AC current, but the inductive loss of the power becomes a major problem when the process is operated at the high frequency for large scale ESR. Nowadays, the demand on large scale ingots has driven the people to think of operating the process with AC current at low frequency. Here the influence of the applied frequency of AC current on the large scale ESR process is numerically investigated. For this purpose, simulations with two operating AC frequencies (0.2 and 50 Hz) are performed. The main goal is to achieve some fundamental understanding of the two-phase flow and the formation of melt pool of the solidifying ingot under the influence of AC frequency. As we also know that the mold current (portion of electric current entering through solid slag skin into the mold) plays an important role in the process, calculations considering different current paths are also analyzed.

Introduction

The aim of the electroslag remelting (ESR) process is purifying and refining steel and other alloys such as Ni-based super alloys. Thermal energy is supplied to the process through the Joule heating that results in remelting the electrode and formation of droplets. The droplets then pass through the slag and reach the liquid pool. The melt pool solidifies directionally and builds the high-grade ingot in a water-cooled mold [1].

In the ESR process the electromagnetic field drives the flow of the molten slag and liquid melt pool, thus the electrical parameters of the process have a significant effect on the quality of the final product. Currently, the ESR process is mostly operating with AC current (50 - 60 Hz) in order to minimize the negative impacts of the electrochemical reactions occurring in the slag.

Comprehensive reviews of electrochemical reactions in the ESR process were presented by Peover and Mitchel [2-3]. In fact, the electric current is conducted by ions in the slag region [4]. Oxidation loss of elements such as Ti, Si, and Al is addressed as a big issue during DC remelting of the electrode in the ESR process [5-7]. The composition fluctuation of elements can significantly reduce the yield strength of the alloys. For instance, a major loss of Ti element (40-80 %) is reported by Etienne in a DC electrode remelting process [5]. Furthermore, the degree of sulphur removal by an ESR process operated with AC current is higher than by an ESR process operated with DC current [8]. Previously, Chang studied experimentally the effect of low frequency AC power supply on qualities of alloy steel [9]. It is generally recognized that the aforementioned alloying phenomena are due to electrochemical reactions taking place at the slag-metal interface when the process is operating with DC or quasi-DC current.

On the other hand, the inductive losses of the power for large scale ESR are the main disadvantage of operating the process at large frequencies. The demand on large scale ingots (diameter > 1 m) has been increased since the last decade. Unfortunately, the inductive losses become more significant as the ingot size increases which are the major drawbacks of applying large frequency for large scale ESR process. Therefore, the industry intends to operate the process at low frequency (0.1 - 5 Hz).

Over the last decades, some efforts were done to model ESR process using CFD [10-12]. Additionally, attempts have been made to investigate the effect of frequency of the applied AC current on the ESR process using numerical simulation. Kharicha studied the effect of the AC electromagnetic field on the flow and slag-pool interfaces [13]. In addition, Liang studied the quality of the ingot for producing GH4169 under different current frequency for a small scale ESR process [14]. Furthermore, Li developed a 3D finite element model (FEM) considering current frequency to simulate the current density, magnetic field, electromagnetic force and Joule heating for the process [15].

In the current work, the influence of the applied frequency of AC power supply for a large scale ESR process using a static mold is investigated. The main goal is to achieve some fundamental understanding of the two-phase flow and the formation of melt pool of the solidifying ingot under the influence of AC frequency.

Numerical Model

In the present study, the Finite Volume Method (FVM) is used for simulation of the fluid flow, heat transfer, and electromagnetic field in the process. The buoyancy and Lorentz forces as well as Joule heating due to the electrical resistance in the whole system are taken into account. The temperature field is obtained by solving the enthalpy conservation equation where Joule heating is added as a source term [16]. The momentum equation is solved to determine the velocity field. The drag resistance of the solidifying dendrites to the flow in the two-phase mushy zone is modeled according to the Black-Kozeny model [17]. Additionally, Lorentz force is added as a source to the momentum equation.

The origin of the Lorentz force is the interaction between the electric current and the self-induced magnetic field in the system. For the sinusoidal AC field, the magnetic field can be expressed using the phasor notation ($B_\theta = \tilde{B}_\theta e^{i\omega t}$) where $\tilde{B}_\theta$ is a function of position. The magnetic field has only azimuthal direction since there is no external magnetic field and the process conditions are axisymmetric. The equation for magnetic field that is derived from the Maxwell's system of equations must be solved in cylindrical coordinate [18]. The equation is given as:

$$\frac{\partial B_\theta}{\partial t}+\left[\frac{\partial}{\partial z}\left(\frac{1}{\sigma\mu_0}\frac{\partial B_\theta}{\partial z}\right)+\frac{\partial}{\partial r}\left(\frac{1}{r\sigma\mu_0}\frac{\partial(rB_\theta)}{\partial r}\right)\right]=0 \quad (1)$$

where μ_0 and σ denote the magnetic permeability and electric conductivity respectively.

After computing the real and imaginary components of the magnetic field, the electric current in the whole system can be obtained using the Ampere's law that is expressed as:

$$\tilde{\vec{j}}=\frac{1}{\mu_0}(\vec{\nabla}\times\tilde{\vec{B}}_\theta) \quad (2)$$

Finally, the time average Lorentz force and Joule heating can be computed:

$$\vec{F}_L=\mathrm{Re}(\frac{1}{2}\vec{j}\times\tilde{\vec{B}}_{\theta\ Conjugate}) \quad (3)$$

$$q_{Joule}=\mathrm{Re}(\frac{1}{2\sigma}\tilde{\vec{j}}\times\tilde{\vec{j}}_{\theta\ Conjugate}) \quad (4)$$

Configuration of the computational domain and boundaries are schematically shown in Figure 1. The computational domain includes the slag and ingot. A 2D axisymmetric calculation is performed. The slag-pool, electrode-slag, and slag-air interfaces are assumed to be flat. The electrode immersion depth is ignored.

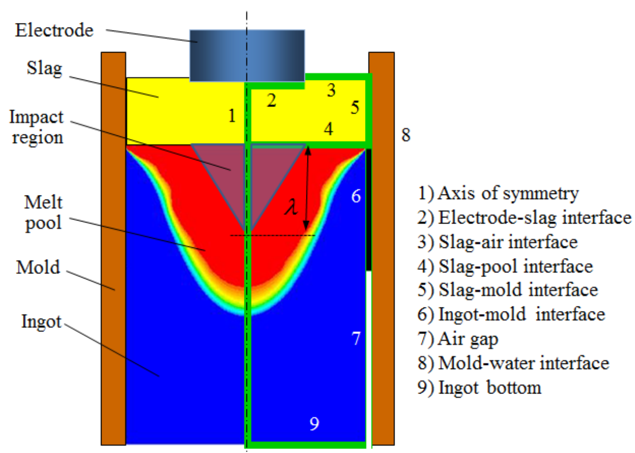

Figure 1: Schematic representation of the computational domain for the ESR process.

The classical way to consider the impact of falling droplets is to use a mass flux of liquid metal at the slag-pool interface [19-20]. Another way of modeling the droplets is prescribing a Gaussian distribution of velocity profile at the interface between the slag and melt pool [18]. In fact, the impact of droplets is not limited only at the surface but deeply inside the melt pool. Therefore, we modify the model considering the impact of droplets by introducing the parameter called impact depth of droplets (λ). With this approach, the droplets are considered to be as the mass, energy, and momentum source carriers which deeply penetrate into the melt pool. The amounts of the sources are assumed to be linearly decreased from the slag-pool interface till the impact depth. The impact depth can be obtained by experiment or direct numerical simulation of droplet–liquid surface splash phenomenon. For our simulations, we assumed that the droplet size is 1 cm and the corresponding impact depth is 15 cm. Furthermore, it is assumed that the droplets enter the pool under the shadow of the electrode.
Non-slip boundary condition is applied for the flow at the electrode-slag interface and at the mold wall, whereas at the slag-pool interface the condition is free-slip. The heat is transferred by convection and radiation between electrode and air, and at the slag-air interface. A value of 0.8 is applied for the emissivity for the mentioned boundaries. The heat is conducted to the mold passing through the slag skin layer from the slag and ingot. In addition, the air gap between the slag skin layer and mold due to shrinkage of solidified ingot is taken into account. The gap alters the thermal boundary condition from the conduction condition to a combined radiation-convection condition. The tip of the electrode (slag-electrode interface) where the droplets form takes the liquidus temperature of the alloy.

In addition, the boundary conditions for the magnetic flux, Eq.(1), are obtained using the Ampere's law. The magnetic induction is prescribed at the slag-air and mould-water interfaces. The continuity of the magnetic induction is applied at the following interfaces: electrode-slag, slag-pool, slag-mold, and ingot-mold. Furthermore, an induction flux of zero is used for the ingot bottom.
Details about the geometry and the average physical properties of the slag and steel are described in Table 1.

Table 1. Parameters used in the simulations.

Steel	
Density (kg·m^{-3})	7100
Viscosity (Kg·m^{-1}·s^{-1})	0.006
Liquidus Temp. (K)	1779
Solidus Temp. (K)	1719
Specific heat, liquid (J·Kg^{-1}·K^{-1})	800
Latent heat of fusion (J·Kg^{-1})	268000
Thermal Conductivity, liquid(W·m^{-1}·K^{-1})	40
Electric Conductivity, liquid(ohm^{-1}·m^{-1})	880000
Slag	
Density (kg·m^{-3})	2800
Viscosity (Kg·m^{-1}·s^{-1})	0.002
Specific heat, liquid (J·Kg^{-1}·K^{-1})	1250
Thermal Conductivity, liquid(W·m^{-1}·K^{-1})	10
Electric Conductivity, liquid(ohm^{-1}·m^{-1})	100
Geometry (Static mold)	
Mold radius (m)	0.9115
Electrode radius (m)	0.725
Slag height (m)	0.265

Several calculations under different operating conditions were performed using the commercial software FLUENT. Table 2 lists the operating conditions for the case studies.

Table 2. Operating conditions of the parameter studies

	RMS current (KA)	Frequency (Hz)	Mold current
Case I	36.5	0.2	No
Case II	36.5	50	No
Case III	36.5	50	Yes

Results

Case I

In Case I a low frequency (0.2 Hz) AC current is applied, and no current enters into mold. Figure 2 (a) shows the temperature field in the whole system and the isolines of solid fraction in the ingot region. The hottest area in the whole system is under the shadow of the slag-air interface.

In fact, an intense vortex forms under the edge of the electrode due to the Lorentz force and buoyancy force. The recirculation of the flow captures the released Joule heat in the slag region. The relative velocity between the melt and the ingot is illustrated in Figure 2 (b). The flow recirculation in the slag region corresponds to the maximum velocity in the whole system. The velocity is predicted to be much smaller in the melt pool than in the slag region. One point needs to be kept in mind is that the slag-pool interface is assumed to be stationary. This assumption would cause underestimation of the flow velocity in the melt pool especially in the vicinity of the slag.

The Lorentz force in the slag and melt pool is shown in Figure 2 (c). It is observed that the Lorentz force is quite homogeneously distributed. Exceptionally, the magnitude of the Lorentz force becomes large near the edge of the electrode. In fact, the variation in the Lorentz force and Joule heating in the slag region is consistent with the current density. Figure 2 (d) shows distributions of the current lines and Joule heating in the process. The maximum amount of Joule heating is released near the edge of the electrode where the current lines are denser. As a matter of fact, the amount of Joule heating is negligible in the electrode and ingot due to low electrical resistance of steel.

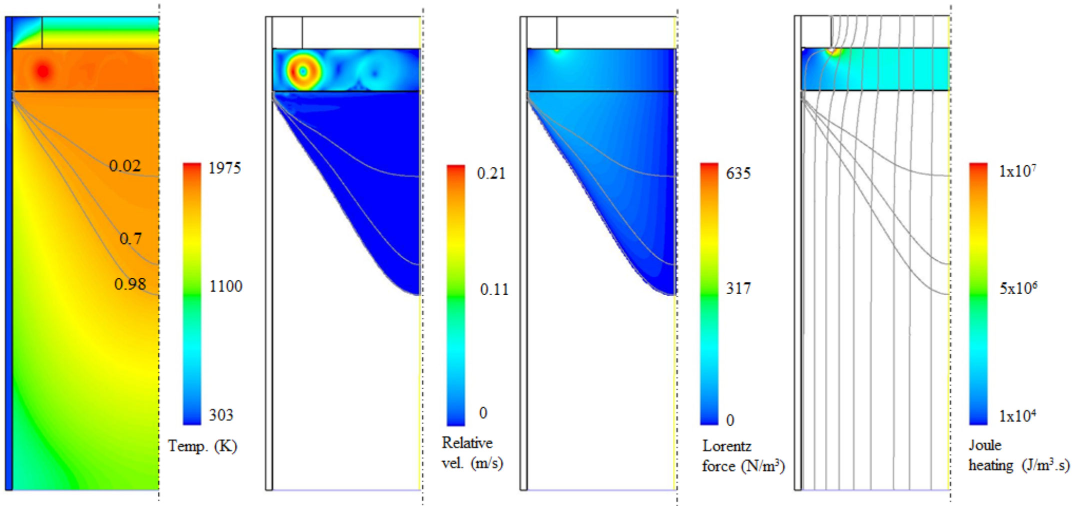

(a) (b) (c) (d)

Figure 2. Contours of (a) the temperature field (b) magnitude of the relative velocity (c) Lorentz force and (d) Joule heating overlaid with the path of electric current for Case I. Isolines of fraction solid (0.02, 0.7 and 0.98) are plotted to indicate the mushy zone.

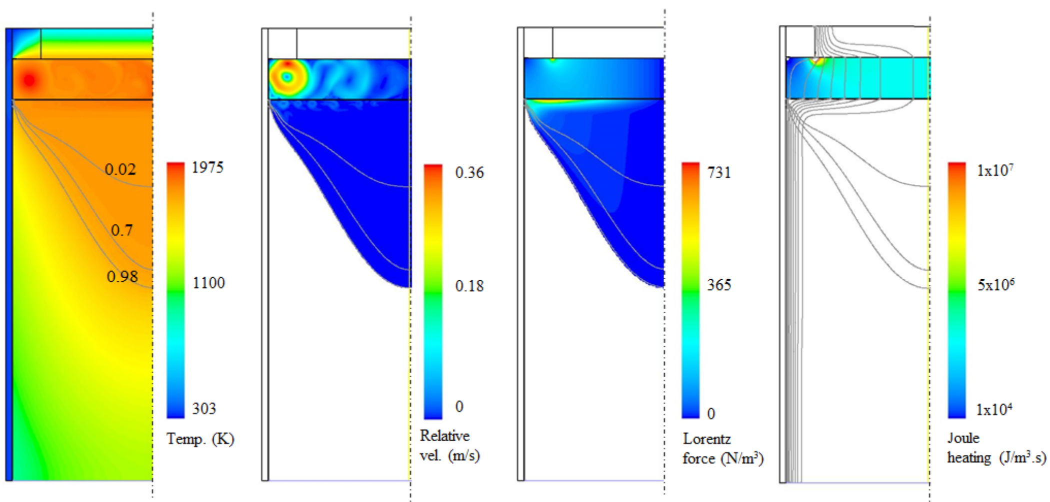

(a) (b) (c) (d)

Figure 3. Contours of (a) the temperature field (b) magnitude of the relative velocity (c) Lorentz force and (d) Joule heating overlaid with the path of electric current for Case II. Isolines of fraction solid (0.02, 0.7 and 0.98) are plotted to indicate the mushy zone.

Case II

Figure 3 shows the contour of temperature, velocity, Lorentz force, and electric current together with Joule heating when the process is run under the frequency of 50 Hz. Again no current enters into mold since the skin layer is assumed to be an insulator. The region where the flow recirculates matches the hottest area in the slag zone as shown in Figure 3 (a). In the slag region, the Lorentz force is quite homogeneously distributed excluding the edge of the electrode where the force is the strongest. For this case, the force gradually increases from the bulk to the region near the mold wall in the melt pool as shown in Figure 3(c).This is due to change of electric current distribution once they enter the melt pool, as shown in Figure 3(d). The electric current flows radially towards the ingot surface as it passes the slag-pool interface. In fact, the electric current tends to flow along the ingot surface because of skin effect.

Case III

Figure 4 shows the modeling results of Case III. This case is same as Case II (50 Hz), but the electric current is allowed to cross the slag skin and enter into the mold.

The thickness of the slag skin layer is assumed to be 1 cm, and the contact length where the current can enter into the mold is 5 cm. Electric conductivities of the liquid slag and the solid slag skin are 100 and 48 respectively. In this case, around 90 % of total current is predicted to pass across the skin layer, as shown in Figure 4 (d). However, only 10 % of the total power is consumed in the skin layer. Due to the special current distribution in this case, strong Lorenz force is predicted in the region near the outer radius region of the slag layer and ingot, and only a very week Lorenz force acting in the bulk of the melt pool, as illustrated in Figure 4 (c).

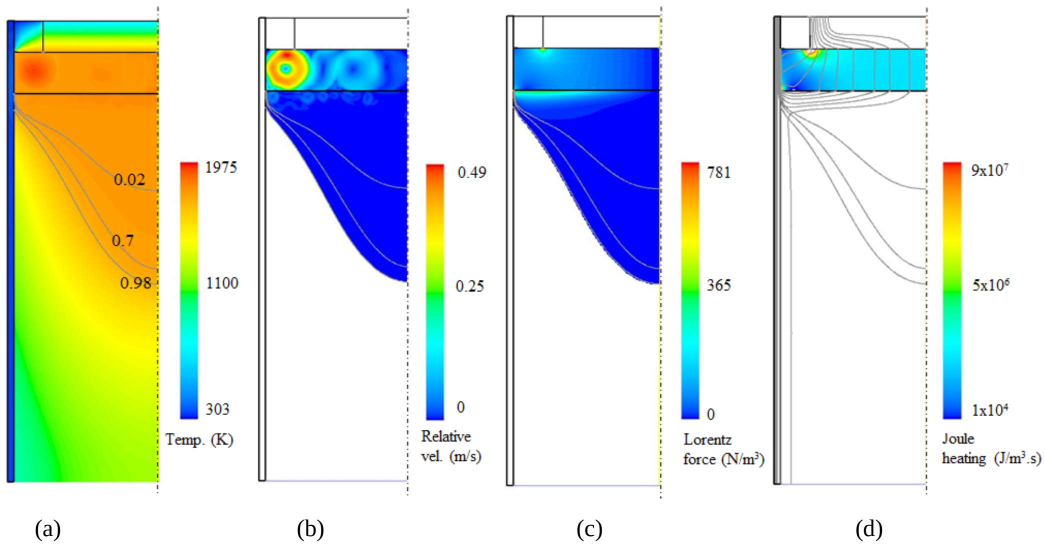

Figure 4. Contours of (a) the temperature field (b) magnitude of the relative velocity (c) Lorentz force and (d) Joule heating overlaid with the path of electric current for Case III. Isolines of fraction solid (0.02, 0.7 and 0.98) are plotted to indicate the mushy zone.

Discussion

The shape of melt pool is an important indicator for the ESR process, and it determines the quality of the as-cast ingot. Parameters of the melt pool (depth, mush zone, standing height) are mainly governed by the global transport phenomena, which are in turn related to the flow intensity of different fluid regions. Intensity of the flow is evaluated by the time-averaged kinetic energy. Influence of the process operating parameters (Case I, II, III) on the average kinetic energy is analyzed (Table 3).

Table 3. Summary of the computed average kinetic energy in different fluid regions.

	Average kinetic energy in slag (J)	Average kinetic energy in melt pool (J)
Case I	6.83	0.03
Case II	23.69	0.096
Case III	56.06	0.186

Effect of frequency

A comparison is made between Case I and Case II to analyze the effect of frequency of AC current as shown in Figure 5. The average kinetic energy in the slag for Case II is larger than that for Case I, see Table 3. It means that the present ESR process run with high frequency has a more severe mixing in the slag region than the process run with low frequency. The more severe the mixing in slag region, the larger the amount of energy being transport into the melt pool. Therefore, with the increase of the current frequency, the pool depth (distance between the slag-pool interface and the isoline of 0.02 solid fraction) is slightly increased. However, the isoline of 0.98 solid fraction moves down that results in thicker mushy zone for Case I than for Case II.

Additionally, the frequency of the AC current can affect the distribution of the Lorentz force at the region near to the slag-melt interface. As shown in Figure 5 (b), the electric current lines have similar distribution at the slag region independent of the applied frequency. Thus, the Lorentz force direction is identical for both cases, that is towards the axis of symmetry. However, at the slag-pool interface the direction is altered for Case II with 50 Hz frequency. It is horizontal and downward, as shown in Figure 6.

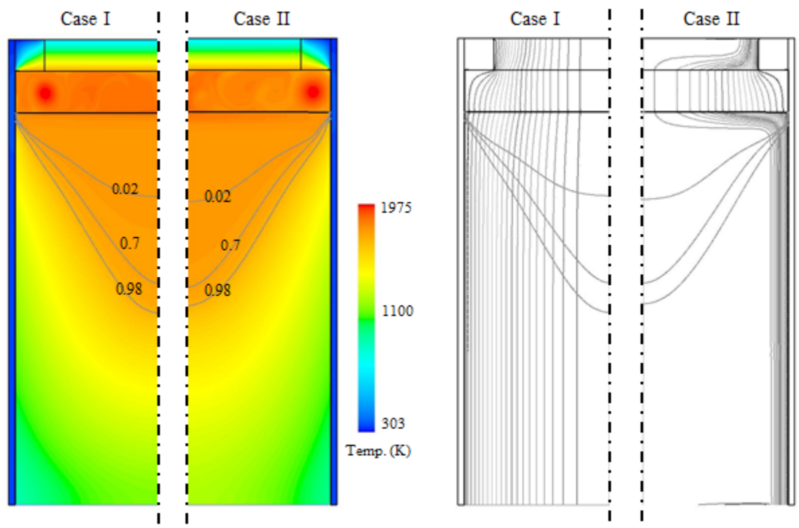

(a) (b)

Figure 5: Influence of the AC current frequency on (a) the temperature field and mushy zone (b) electric current distribution. Two cases are compared: Case I with frequency of 0.2 Hz: Case II with frequency of 50 Hz.

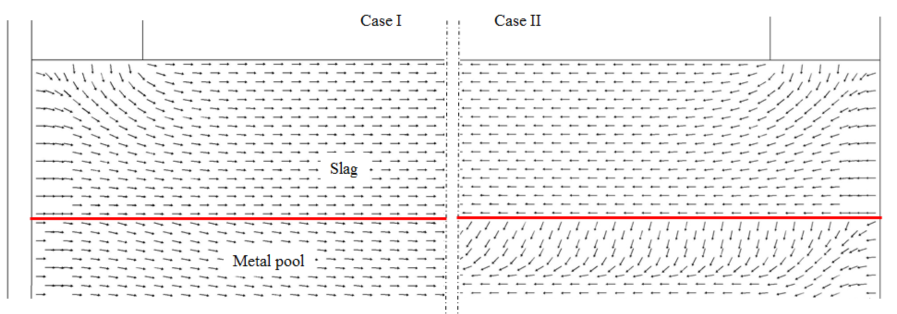

Figure 6: Influence of the AC current frequency on the direction of the Lorentz force, Two cases are compared: Case I with frequency of 0.2 Hz: Case II with frequency of 50 Hz.

Effect of mold current

Here, Case II and Case III are compered to study the influence of mold current on the pool shape, as illustrated in Figure 7. The average kinetic energy in the slag and melt pool is much larger for Case III than for Case II. Accordingly, the bulk of the slag is severely mixed in Case III with mold current. This mixing promotes the transfer of heat from slag to melt pool, hence leads to a raise of the melt pool temperature and a deeper pool.

The electric current lines are shown in Figure7 (b). For Case III a huge amount (92%) of the current enters into the mold in the region close to slag-pool interface where there is still contact between the metal and mold. This changes the pattern of the flow in this region, and results in larger standing height of the melt pool than for Case II without mold current. In addition, the skin effect in the copper mold is significant. Inside the mold the electric current only flows near the mold surfaces, as shown in Figure 7(b).

At high frequency, the current density and consequently the Lorentz force is week in the bulk of the melt pool where the flow is mainly driven by buoyancy. The direction of the Lorentz force is compared to study the effect of the mold current on the flow, as indicated in Figure 8. The direction of the Lorentz force is similar in the slag region and slag-pool interface in the central part of the system. However, for Case III with the mold current, the direction of the Lorentz force bents downwards near the mold wall both in the slag and melt pool regions. The Lorentz force and buoyancy act in the same direction and the flow is pushed downwards. The downward flow near the mold wall increases the standing height of the melt pool. The standing height is defined as the distance from the slag-pool interface to the start of solidification at the ingot surface (as shown in Figure 7a).

Joule heat is uniformly released under the electrode for both cases as shown in Figure 9. However, for Case II inhomogeneous distribution of Joule heat is released along the slag-mold interface. The minimum heat source is noticed near the slag-air interface for Case II where the slag skin layer acts as an electric insulator. In contrast, the magnitude of Joule heat source is significantly large at this region for Case III with mold current. Since this area is closer to the edge of the electrode, the electric resistance drops and more current flows through it. In the vicinity of the slag-pool interface Joule heating is pretty large for case III. This region is the most favorable path for the electric current to flow.

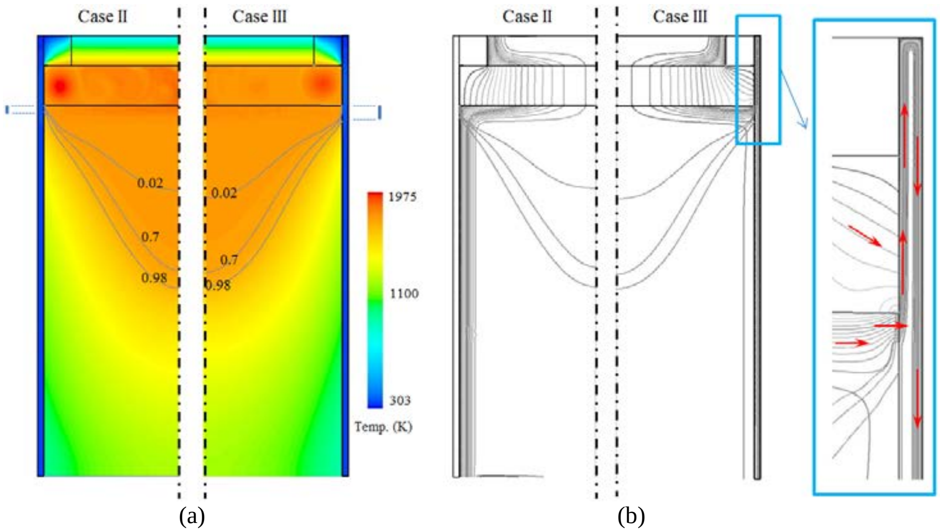

Figure 7: Influence of the mold current (frequency of 50 Hz) on (a) the temperature field and mushy zone (distance between dotted lines indicates the standing height) (b) electric current path (red arrows indicate the direction of electric current). Two cases are compared: Case II without mold current: Case III with mold current.

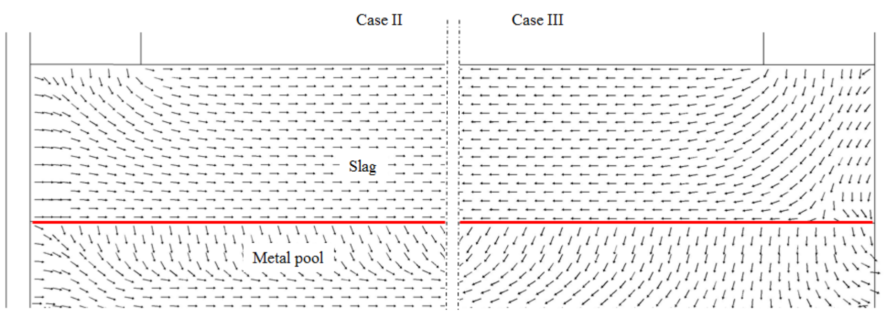

Figure 8: Influence of the mold current (frequency of 50 Hz) on the direction of the Lorentz force. Two cases are compared: Case II without mold current: Case III with mold current.

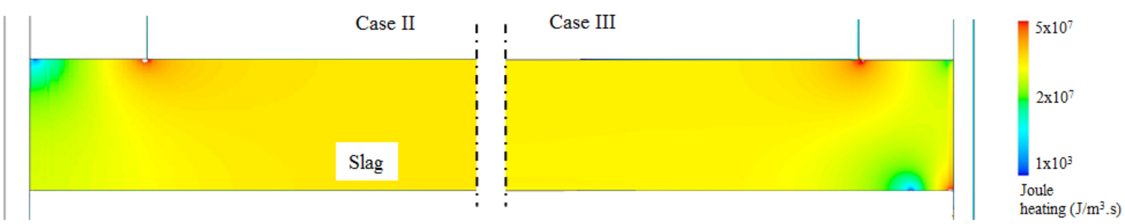

Figure 9: Influence of the Mold current (frequency of 50 Hz) on the distribution of the Joule heating, Two cases are compared: Case II without mold current: Case III with mold current.

<u>Validity of the modeling result</u>

A 2D axisymmetric model is used to solve the governing equations of electromagnetic field, heat transfer, and flow of the ESR process. The model is robust and computationally efficient to study the influence of electrical parameters on the solidification of the ingot. It is observed that the electrical parameters such as electric conductivity and frequency of the applied AC current have a huge influence on the shape of the melt pool. The electric conductivities of the slag (liquid and solid) are the main properties determining the electric current path, hence influencing other quantities of the process. As such properties are assumed, the current study is considered to be preliminary and qualitative. Some other factors influencing the quantitative accuracy of the modeling results should be kept in mind for improving the future model: the forming metal droplets under the electrode would adapt the electromagnetic field to a certain extend [21]; the motion of the slag-pool interface can affect the flow, temperature and electromagnetic fields of the system [22]; the nature of the flow in the real process is in 3D, but the current calculation can only be performed in 2D; the turbulence of the flow which is ignored would enhance the global energy transfer as well. In spite of the model simplifications, which are necessary at the current stage, the performed parameter studies in this paper can provide valuable information about the qualitative influence of the process parameters on some key solidification quantities of the ingot, such as the shape and depth of the melt pool, standing height, mushy zone, etc.

Summary

The influence of the applied frequency of AC current on the large scale ESR process with static mold has been numerically investigated. Main findings are summarized as follows.

- The melt pool shape of the solidifying ingot is slightly influenced by the applied frequency.
- In the case of high AC frequency, due to the skin effect, the current path changes its direction when the current passes the slag-pool interface, and so does the Lorenz force. As a consequence, it influences the hydrodynamic behavior of the slag and melt pool near the slag-pool interface.
- The distribution patterns of Joule heating and Lorentz force in the slag region are quite independent of the applied frequency in the slag region.

Additionally, the effect of the mold current (allow current entering into mold) is also considered. We found:

- Distribution patterns of the Lorentz force and Joule heating in the slag region are significantly influenced by the mold current, especially near the mold wall.
- Mold current promotes stirring in the slag region.
- Mold current increases the standing height of the melt pool.

Acknowledgements

The authors acknowledge the financial support by the Austrian Federal Ministry of Economy, Family and Youth and the National Foundation for Research, Technology and Development.

References

1. G. Hoyle, *Electroslag Processes* (London, Applied Science Publishers, 1983).
2. M.E. Peover, "Electroslag remelting, a review of electrical and electrochemical aspects," *J. Inst. Metals*, 100 (1972), 97-106.
3. A. Mitchell and G. Beynon, "Electrode polarization in the DC electroslag melting of pure iron," *Met. Trans B*, 10 (1971), 3333-3345.
4. Y. Kojima, M. Kato, T. Toyoda, and M. Inouye, "The formation of liquid droplet and behavior of oxygen in direct current electroslag remelting process," *ISIJ*, 15 (1975), 397-406.
5. M. Etienne, "The loss of reactive elements during electroslag processing of iron-base alloys," (Ph.D. Thesis, University of British Columbia, 1970).
6. G.K. Bhat and A. Mitchell, *Proc. Sec. Symp. On ESR technology*, Part I (1969).
7. B.I. Medovar, *Electroslag remelting* (Moscow, House of Literature on Ferrous and Nonferrous Metallurgy, 1963).
8. D.A. Whittaker, (Ph.D. Thesis, McMaster University, 1968).
9. L. Chang, X. Shi, H. Yang, Z. Li, "Effect of low-frequency AC power supply during electroslag remelting on qualities of alloy steel," *J. of Iron and Steel Research*, 16 (4) (2009), 7-11.
10. V. Weber, A. Jardy, B. Dussoubs, D. Ablitzer, S. Ryberon, V. Schmitt, S. Hans, H. Poisson, "A comprehensive model of the electroslag remelting process: description and validation," *Proc. of LMPC*, Nancy, 2007, 83-88.
11. Z. Jiang and Y. Dong, "Solidification model for electroslag remelting process," *Proc. of LMPC*, Nancy, 2007, 89-94.
12. Matthew J. M. Krane, Michael Fahrmann, Jeff Yanke, Enrique Escobar de Obaldia, Kyle Fezi, and Jonathan Busch, "A comparison of predictions of transport phenomena in electroslag remelting to industrial data," *Proc. of LMPC*, Nancy, 2011, 65-72.
13. A. Kharicha, M. Wu, A. Ludwig, B. Ofner, and H. Holzgruber, *CFD Modeling and simulation in materials processing* (US, Wiley publication, 2012), 139.
14. Q. Liang, X. Chen, H. Ren, C. Shi, and H. Guo, "Numerical simulation of electroslag remelting process for producing GH4169 under different current frequency," *Adv. Materials Research*, (482-484)(2012), 1556-1565.
15. B. Li, F. Wang, and F. Tsukihashi, "Current, magnetic field and joule heating in electroslag remelting processes," *ISIJ Int.*, 52 (7) (2012), 1289-1295.
16. A. Kharicha, W. Schützenhöfer, A. Ludwig, and R. Tanzer, "Numerical and experimental investigations on the ESR process of the hot work tool steel H11," *Proc. of LMPC*, Santa Fe, 2009, 235-242.
17. V. R. Voller, and C. Prakash, "A fixed grid numerical modeling methodology for convection-diffusion mushy region phase-change problems," *Int. J. Heat Mass Transfer*, 30(8) (1987), 1709-1719.
18. A. Kharicha, W. Schützenhöfer, A. Ludwig, and R. Tanzer, "Selected numerical investigations on ESR process," *Proc. of LMPC*, Nancy, 2007, 113-119.
19. A. H. Dilawari, and J. Szekely,"Heat transfer and fluid flow phenomena in electroslag refining," *Metall. Trans. B*, 9B (1) (1975), 77-87.
20. M. Choudhary, and J. Szekely, "Modeling of fluid flow and heat transfer in industrial-scale ESR system," *Ironmaking Steelmaking*, 8(5) (1981), 225-239.
21. A. Kharicha, A. Ludwig, M. Wu, "Droplet formation in small electroslag remelting processes," *Proc. of LMPC*, Nancy, 2011, 113-119.
22. A. Kharicha, A. Ludwig, M. Wu, "3D simulation of the melting during an industrial scale electro-slag remelting process," *Proc. of LMPC*, Nancy, 2011, 41-48.